

# Accessible ring opening metathesis and atom transfer radical polymerization catalysts based on dimethyl sulfoxide ruthenium(II) complexes bearing *N*-heterocyclic carbene ligands

André H.S. Idehara<sup>a</sup>, Patrik D.S. Gois<sup>a</sup>, Henrique Fernandez<sup>b</sup>, Beatriz E. Goi<sup>a</sup>, Antonio E.H. Machado<sup>c</sup>, Benedito S. Lima-Neto<sup>b</sup>, Valdemiro P. Carvalho Jr.<sup>a,\*</sup>

<sup>a</sup> Faculdade de Ciências e Tecnologia, UNESP Univ Estadual Paulista, CEP 19060-900, Presidente Prudente, SP, Brazil

<sup>b</sup> Instituto de Química de São Carlos, Universidade de São Paulo, CEP 13560-970, São Carlos, SP, Brazil

<sup>c</sup> Instituto de Química, UFU Universidade Federal de Uberlândia, CEP 38400-902, Uberlândia, MG, Brazil

## ARTICLE INFO

### Keywords:

Ruthenium complexes  
ROMP  
ATRP  
Norbornene  
Methyl methacrylate

## ABSTRACT

Dimethyl sulfoxide ruthenium(II) complexes of *N*-heterocyclic carbenes derived from cycloalkylamines (cyclopentyl (**1a**), cyclohexyl (**1b**), cycloheptyl (**1c**), and cyclooctyl (**1d**)) were synthesized: [RuCl<sub>2</sub>(S-dmsO)<sub>2</sub>(IPent)] (**2a**), [RuCl<sub>2</sub>(S-dmsO)<sub>2</sub>(IHex)] (**2b**), [RuCl<sub>2</sub>(S-dmsO)<sub>2</sub>(IHept)] (**2c**), and [RuCl<sub>2</sub>(S-dmsO)<sub>2</sub>(IOct)] (**2d**). The imidazolium salts **1a-1d** were characterized by FTIR, UV-vis, and <sup>1</sup>H and <sup>13</sup>C NMR spectroscopy, while their respective dimethyl sulfoxide ruthenium(II) complexes (**2a-2d**) were characterized by elemental analysis, FTIR, UV-vis, <sup>1</sup>H and <sup>13</sup>C NMR, and cyclic voltammetry. The complexes **2a-2d** were evaluated as catalytic precursors for ROMP of norbornene (NBE) and for ATRP of methyl methacrylate (MMA). The polynorbornene (polyNBE) syntheses via ROMP using the complexes **2a-2d** as pre-catalysts were evaluated under reaction conditions of [EDA]/[Ru] = 28 (5 μL), [NBE]/[Ru] = 5000 at 50 °C as a function of time. The polymerization of MMA via ATRP was conducted using the complexes **2a-2d** in the presence of ethyl 2-bromoisobutyrate (EBiB) as the initiator. All tests were using the molar ratio [MMA]/[EBiB]/[Ru] = 1000/2/1 and conducted at 85 °C. The linear correlation of ln([MMA]<sub>0</sub>/[MMA]) and time clearly indicates that the concentration of radicals remains constant during the polymerization and that the ATRP of MMA mediated by **2a-2d** proceeds in a controlled manner.

## 1. Introduction

Organometallic catalysts are designed and optimized to mediate a single reaction [1]. As the number of applications that require combinatorial synthetic protocols increases [2,3], it will become desirable for catalysts to mediate multiple, mechanistically distinct transformations directly or upon simple modification.

The preparation of new polymeric materials composed of segments that cannot be prepared by the same polymerization mechanism remains a challenge in synthetic polymer chemistry. Thus, many new strategies have emerged which are based on using substrates that are capable of initiating more than one type polymerization. While a few of these protocols permit the combination of all the desired monomers at the beginning of the polymerization, the majority require timed additions [4–9]. Furthermore, a number of organometallic complexes and co-catalysts must be included to control the polymerizations. Ultimately, it is desirable to develop new catalytic systems that have the

ability to mediate several mechanistically different transformations, either directly or by simple modification; therefore requiring only the addition of desired monomers [10].

The ruthenium-based catalyst systems have been demonstrated to be effective for initiating the ring-opening metathesis polymerization (ROMP) of a variety of cyclic olefins and as mediators for atom-transfer radical polymerization (ATRP) of vinyl monomers [11–16]. The Grubbs' ruthenium benzylidene, Cl<sub>2</sub>(PCy<sub>3</sub>)<sub>2</sub>Ru = CHPh, known as a very active olefin metathesis catalyst, showed to be also capable of performing ATRP of styrene and methyl methacrylates [17].

In light of these observations, we became interested in the development of Ru catalysts that can do both ROMP and ATRP reactions. During the past 15 years, easy and efficient synthesis of ruthenium-based ROMP catalysts has been developed by our group [18–24]. Recently, some of the complexes have been successfully applied to controlled/living radical polymerizations of vinyl monomers [25–27].

Herein, for the first time, we report the facile preparation and

\* Corresponding author.

E-mail address: [valdemiro@fct.unesp.br](mailto:valdemiro@fct.unesp.br) (V.P. Carvalho).

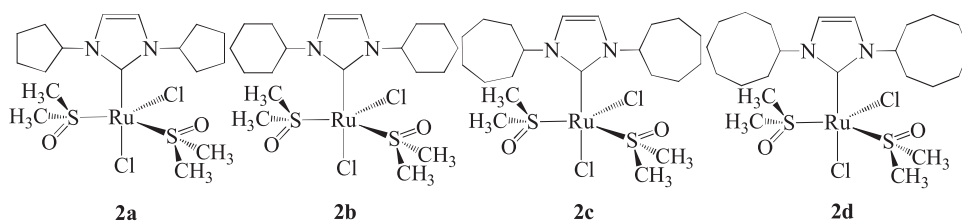


Fig. 1. Illustration of the NHC ruthenium(II) complexes 2a–2d.

evaluation of dimethyl sulfoxide-ruthenium(II) complexes bearing NHC ligands substituted with cycloalkyl groups: cyclopentyl (**2a**), cyclohexyl (**2b**), cycloheptyl (**2c**), and cyclooctyl (**2d**) (Fig. 1), as catalyst precursors for ROMP of norbornene (NBE) and ATRP of methyl methacrylate (MMA). Ethyl diazoacetate (EDA) was used as carbene source for ROMP and ethyl 2-bromoisobutyrate (EBiB) was used as initiator for ATRP. The goal was to observe the influence of cycloalkyl groups and its effects on catalytic activity of the studied complexes, discussing the  $\sigma$ -donor ability and steric hindrance, obtaining resources to understand the factors that influence the efficiency of both reactions.

## 2. Experimental

### 2.1. General remarks

Unless otherwise stated, all syntheses and manipulations were performed under nitrogen atmosphere following standard Schlenk techniques. Solvents were distilled from appropriate drying agents and deoxygenated prior to use. Methyl methacrylate (MMA) was washed with 5% NaOH solution, dried over anhydrous  $\text{MgSO}_4$ , vacuum distilled from  $\text{CaH}_2$  and stored under nitrogen at  $-18^\circ\text{C}$  before use. Glyoxal (40% aqueous solution) was stored in a cold room at  $+4^\circ\text{C}$ .  $\text{RuCl}_3 \cdot x\text{H}_2\text{O}$ , 2,2,6,6-tetramethyl-1-piperidinoxyl (TEMPO), tetrabutylammonium hexafluorophosphate ( $n\text{-Bu}_4\text{NPF}_6$ ), ferrocene (Fc), norbornene (NBE), ethyl diazoacetate (EDA), cyclopentylamine, cyclohexylamine, cycloheptylamine, cyclooctylamine, paraformaldehyde, tetrafluoroboric acid, dimethylsulfoxide, and ethyl 2-bromoisobutyrate (EBiB) were obtained from Aldrich and used as acquired. The  $[\text{RuCl}_2(\text{S-dms})_3(\text{O-dms})]$  complex was prepared following the literature and its purity was checked by satisfactory elemental analysis and spectroscopic examination (NMR, FTIR, and EPR) [28].

### 2.2. Analyses

Elemental analyses were performed with a Perkin-Elmer CHN 2400 at the Elemental Analysis Laboratory of Institute of Chemistry – USP. ESR measurements from solid sample were conducted at 77 K using a Bruker ESR 300C apparatus (X-band) equipped with a TE102 cavity and an HP 52152A frequency counter. The FTIR spectra were obtained on a Bomem FTIR MB 102. Electronic spectra were recorded on a Shimadzu (model UV-1800) spectrophotometer, using 1 cm path length quartz cells. The  $^1\text{H}$  and  $^{13}\text{C}$  NMR spectra were obtained in  $\text{CDCl}_3$  at 298 K on a Bruker DRX-400 spectrometer operating at 400.13 and 100.62 MHz, respectively. Chemical shifts are listed in parts per million downfield from TMS and are referenced from the solvent peaks or TMS. Conversion was determined from the concentration of residual monomer measured by gas chromatography (GC) using a Shimadzu GC-2010 gas chromatograph equipped with a flame ionization detector and a 30 m (0.53 mm I.D., 0.5  $\mu\text{m}$  film thickness) SPB-1 Supelco fused silica capillary column. Anisole was added to polymerization and used as an internal standard. Analysis conditions: injector and detector temperature,  $250^\circ\text{C}$ ; temperature program,  $40^\circ\text{C}$  (4 min),  $20^\circ\text{C min}^{-1}$  until  $200^\circ\text{C}$ ,  $200^\circ\text{C}$  (2 min). The molecular weights and the molecular weight distribution of the polymers were determined by gel permeation chromatography using a Shimadzu Prominence LC system equipped with a LC-20AD pump, a DGU-20A5 degasser, a CBM-20A

communication module, a CTO-20A oven at  $40^\circ\text{C}$  and a RID-10A detector equipped with two Shimadzu column (GPC-805: 30 cm,  $\varnothing = 8.0$  mm). The retention time was calibrated with standard mono-dispersed polystyrene using HPLC-grade THF as an eluent at  $40^\circ\text{C}$  with a flow rate of  $1.0 \text{ mL min}^{-1}$ . Electrochemical measurements were performed using an Autolab PGSTAT204 potentiostat with a stationary platinum disk and a wire as working and auxiliary electrodes, respectively. The reference electrode was Ag/AgCl. The measurements were performed at  $25^\circ\text{C} \pm 0.1$  in  $\text{CH}_2\text{Cl}_2$  with  $0.1 \text{ mol L}^{-1}$  of  $n\text{-Bu}_4\text{NPF}_6$ .

### 2.3. General procedure for the preparation of N-heterocyclic ligands

To prepare the N-heterocyclic carbenes (NHC) ligands **1a–1d**, a 50 mL round-bottom flask equipped with a magnetic stirring bar and a stopper was charged with cycloalkylamine (10 mmol), toluene (10 mL), and paraformaldehyde (10 mmol). The resulting milky suspension was stirred for 30 min at room temperature until the solid was almost completely dissolved. The mixture was cooled to  $0^\circ\text{C}$  in an ice/water bath and a second equivalent of cycloalkylamine (10 mmol) was added. The resulting yellow solution was stirred for 10 min at  $0^\circ\text{C}$  before tetrafluoroboric acid (48% aqueous solution, 12.5 mmol) was added portionwise in 15 min. The cooling bath was removed and glyoxal (40% aqueous solution, 10 mmol) was added. The resulting cloudy mixture was stirred overnight (ca. 12 h) in an oil bath at  $50^\circ\text{C}$ . After cooling to room temperature, dichloromethane (10 mL) and water (20 mL) were added and the layers were separated. The aqueous phase was extracted with 3 portions of dichloromethane (10 mL each). The organic layers were combined and dried over  $\text{MgSO}_4$ . After evaporation of the solvent, the beige residue was recrystallized from isopropanol to afford pure 1,3-dicycloalkylimidazolium tetrafluoroborate.

#### 2.3.1. 1,3-dicyclopentylimidazolium tetrafluoroborate **1a**

Paraformaldehyde (0.4 g, 10.0 mmol), cyclopentylamine (2.0 mL, 20.0 mmol), glyoxal (1.1 mL, 10 mmol), and tetrafluoroboric acid (1.1 g, 12.5 mmol) afforded 1.27 g (67%) of the title compound as white needles. (a) UV–vis:  $\lambda_{\text{max}(n)}$  (nm),  $\epsilon_{\text{max}(n)}$  [ $\text{M}^{-1} \text{cm}^{-1}$ ]:  $\lambda_{\text{max}(1)}$  (241 nm),  $\epsilon_{\text{max}(1)}$  [3200];  $\lambda_{\text{max}(2)}$  (324),  $\epsilon_{\text{max}(2)}$  [1200];  $\lambda_{\text{max}(3)}$  (374),  $\epsilon_{\text{max}(3)}$  [670]; (b) FTIR (KBr):  $\nu_x$  ( $\text{cm}^{-1}$ ):  $\nu_{\text{C}=\text{C}}$  (1562),  $\nu_{\text{C}=\text{N}}$  (1634),  $\nu_{\text{C}-\text{H}}$  (2934); (c)  $^1\text{H}$  NMR (400 MHz,  $\text{CDCl}_3$ ):  $\delta = 8.93$  (s, 1H, CH Im), 7.40 (s, 2H,  $\text{CH}_{4,5}$  Im), 4.79 (m, 2H, NCH), 2.34 (m, 4H,  $\text{CH}_2^{\text{Pentyl}}$ ), 1.89 (m, 8H,  $\text{CH}_2^{\text{Pentyl}}$ ), 1.76 (m, 4H,  $\text{CH}_2^{\text{Pentyl}}$ ).  $^{13}\text{C}$  NMR (100 MHz,  $\text{CDCl}_3$ ):  $\delta = 134.3$  ( $\text{CH}^2$  Im), 120.8 ( $\text{CH}^{4,5}$  Im), 61.5 ( $\text{CH}^{\text{Pentyl}}$ ), 33.2 ( $\text{CH}_2^{\text{Pentyl}}$ ), 23.7 ( $\text{CH}_2^{\text{Pentyl}}$ ) ppm.

#### 2.3.2. 1,3-dicyclohexylimidazolium tetrafluoroborate **1b**

Paraformaldehyde (0.4 g, 10.0 mmol), cyclohexylamine (2.3 mL, 20.0 mmol), glyoxal (1.1 mL, 10 mmol), and tetrafluoroboric acid (1.1 g, 12.5 mmol) afforded 1.5 g (64%) of the title compound as white needles. (a) UV–vis:  $\lambda_{\text{max}(n)}$  (nm),  $\epsilon_{\text{max}(n)}$  [ $\text{M}^{-1} \text{cm}^{-1}$ ]:  $\lambda_{\text{max}(1)}$  (241),  $\epsilon_{\text{max}(1)}$  [3180];  $\lambda_{\text{max}(2)}$  (282),  $\epsilon_{\text{max}(2)}$  [1780];  $\lambda_{\text{max}(3)}$  (325),  $\epsilon_{\text{max}(3)}$  [1650]; (b) FTIR (KBr):  $\nu_x$  ( $\text{cm}^{-1}$ ):  $\nu_{\text{C}=\text{C}}$  (1559),  $\nu_{\text{C}=\text{N}}$  (1635),  $\nu_{\text{C}-\text{H}}$  (2928); (c)  $^1\text{H}$  NMR (400 MHz,  $\text{CDCl}_3$ ):  $\delta = 8.92$  (s, 1H,  $\text{CH}^2$  Im), 7.47 (s, 2H,  $\text{CH}^{4,5}$  Im), 4.35–4.29 (m, 2H, NCH), 2.19–2.16 (m, 4H,  $\text{CH}_2^{\text{Hexyl}}$ ), 1.92–1.89 (m, 4H,  $\text{CH}_2^{\text{Hexyl}}$ ), 1.74–1.67 (m, 6H,  $\text{CH}_2^{\text{Hexyl}}$ ), 1.52–1.42 (m, 4H,  $\text{CH}_2^{\text{Hexyl}}$ ), 1.33–1.25 (m, 2H,  $\text{CH}_2^{\text{Hexyl}}$ ) ppm.  $^{13}\text{C}$  NMR (100 MHz,  $\text{CDCl}_3$ ):  $\delta = 133.0$  ( $\text{CH}_2$  Im), 120.5 ( $\text{CH}_{4,5}$  Im), 60.1

(CH<sup>Hexyl</sup>), 33.3 (CH<sub>2</sub><sup>Hexyl</sup>), 25.0 (CH<sub>2</sub><sup>Hexyl</sup>), 24.6 (CH<sub>2</sub><sup>Hexyl</sup>) ppm. These NMR data matched those reported in the literature.[29,30]

### 2.3.3. 1,3-dicycloheptylimidazolium tetrafluoroborate **1c**

Paraformaldehyde (0.4 g, 10.0 mmol), cycloheptylamine (2.6 mL, 20.0 mmol), glyoxal (1.1 mL, 10 mmol), and tetrafluoroboric acid (1.1 g, 12.5 mmol) afforded 0.91 g (72%) of the title compound as white needles. (a) UV-vis:  $\lambda_{\max(n)}$  (nm),  $\epsilon_{\max(n)}$  [M<sup>-1</sup> cm<sup>-1</sup>]:  $\lambda_{\max(1)}$  (241 nm),  $\epsilon_{\max(1)}$  [3195];  $\lambda_{\max(2)}$  (325),  $\epsilon_{\max(2)}$  [720];  $\lambda_{\max(3)}$  (364),  $\epsilon_{\max(3)}$  [581]; (b) FTIR (KBr):  $\nu_x$  (cm<sup>-1</sup>):  $\nu_{C=C}$  (1552),  $\nu_{C=N}$  (1630),  $\nu_{C-H}$  (2921); (c) <sup>1</sup>H NMR (400 MHz, CDCl<sub>3</sub>):  $\delta$  = 8.95 (s, 1H, CH Im), 7.38 (s, 2H, CH<sub>4,5</sub> Im), 4.47 (m, 2H, NCH), 2.14 (m, 4H, CH<sub>2</sub><sup>Heptyl</sup>), 1.92 (m, 4H, CH<sub>2</sub><sup>Heptyl</sup>), 1.78 (m, 5H, CH<sub>2</sub><sup>Heptyl</sup>), 1.62 (m, 12H, CH<sub>2</sub><sup>Heptyl</sup>) ppm. <sup>13</sup>C NMR (100 MHz, CDCl<sub>3</sub>):  $\delta$  = 133.2 (CH<sup>2</sup> Im), 120.3 (CH<sup>4,5</sup> Im), 62.5 (CH<sup>Heptyl</sup>), 35.7 (CH<sub>2</sub><sup>Heptyl</sup>), 27.0 (CH<sub>2</sub><sup>Heptyl</sup>), 24.0 (CH<sub>2</sub><sup>Heptyl</sup>) ppm.

### 2.3.4. 1,3-dicyclooctylimidazolium tetrafluoroborate **1d**

Paraformaldehyde (0.4 g, 10.0 mmol), cyclooctylamine (2.8 mL, 20.0 mmol), glyoxal (1.1 mL, 10 mmol), and tetrafluoroboric acid (1.1 g, 12.5 mmol) afforded 0.88 g (74%) of the title compound as white needles. (a) UV-vis:  $\lambda_{\max(n)}$  (nm),  $\epsilon_{\max(n)}$  [M<sup>-1</sup> cm<sup>-1</sup>]:  $\lambda_{\max(1)}$  (244 nm),  $\epsilon_{\max(1)}$  [3860];  $\lambda_{\max(2)}$  (316),  $\epsilon_{\max(2)}$  [2810];  $\lambda_{\max(3)}$  (380),  $\epsilon_{\max(3)}$  [1890]; (b) FTIR (KBr):  $\nu_x$  (cm<sup>-1</sup>):  $\nu_{C=C}$  (1558),  $\nu_{C=N}$  (1644),  $\nu_{C-H}$  (2923); (c) <sup>1</sup>H NMR (400 MHz, CDCl<sub>3</sub>):  $\delta$  = 8.94 (s, 1H, CH Im), 7.29 (s, 2H, CH<sub>4,5</sub> Im), 4.54 (m, 2H, NCH), 1.98 (m, 8H, CH<sub>2</sub><sup>Octyl</sup>), 1.72 (m, 5H, CH<sub>2</sub><sup>Octyl</sup>), 1.57 (m, 15H, CH<sub>2</sub><sup>Octyl</sup>) ppm. <sup>13</sup>C NMR (100 MHz, CDCl<sub>3</sub>):  $\delta$  = 133.7 (CH<sub>2</sub> Im), 120.3 (CH<sub>4,5</sub> Im), 61.7 (CH<sup>Octyl</sup>), 33.5 (CH<sub>2</sub><sup>Octyl</sup>), 26.3 (CH<sub>2</sub><sup>Octyl</sup>), 25.4 (CH<sub>2</sub><sup>Octyl</sup>), 23.8 (CH<sub>2</sub><sup>Octyl</sup>) ppm.

## 2.4. General procedure for the preparation of NHC-Ru complexes

An oven-dried 100 mL round-bottom flask equipped with a magnetic stirring bar and capped with a three-way stopcock was charged with an 1,3-dicycloalkylimidazolium tetrafluoroborate (**1a-1d**) (1 equiv), 95% sodium hydride (1.2 equiv) and a catalytic amount of potassium *tert*-butoxide. The reactor was purged of air by applying three vacuum/argon cycles before dry THF was added. The resulting suspension was stirred 2 h at room temperature, it was then allowed to settle for 1 h. The supernatant solution was filtered through Celite and transferred with a cannula under inert atmosphere into a two neck 100 mL round-bottom flask equipped with a magnetic stirring bar and capped with a three-way stopcock containing a solution of [RuCl<sub>2</sub>(S-dmsO)<sub>3</sub>(O-dmsO)] (1 equiv) in dichloromethane (10 mL). After 4 h of stirring at room temperature, the solvent was evaporated under vacuum. The residue was washed with *n*-pentane (20 mL). It was dried under high vacuum and recrystallized by slow diffusion of pentane into concentrated dichloromethane solution of the complex.

### 2.4.1. Complex **2a**

[RuCl<sub>2</sub>(S-dmsO)<sub>3</sub>(O-dmsO)] complex (350 mg, 0.72 mmol), NHC **1a** (205 mg, 1 mmol), and THF (50 mL) afforded 368 mg (84%) of the title complex as a yellow solid: anal. calculated for C<sub>17</sub>H<sub>32</sub>Cl<sub>2</sub>N<sub>2</sub>O<sub>2</sub>RuS<sub>2</sub> was 38.34C, 6.07H and 5.26% N; found: 38.45C, 6.23H and 5.12% N. (a) UV-vis:  $\lambda_{\max(n)}$  (nm),  $\epsilon_{\max(n)}$  [M<sup>-1</sup> cm<sup>-1</sup>]:  $\lambda_{\max(1)}$  (243),  $\epsilon_{\max(1)}$  [4837];  $\lambda_{\max(2)}$  (330),  $\epsilon_{\max(2)}$  [389]; (b) FTIR (CsI):  $\nu_x$  (cm<sup>-1</sup>):  $\nu_{C=C}$  (1552),  $\nu_{C=N}$  (1649),  $\nu_{S=O}$  (1102, 1022),  $\nu_{Ru-S}$  (428); (c) <sup>1</sup>H NMR (400 MHz, CDCl<sub>3</sub>):  $\delta$  = 7.20 (s, 1H, CH<sub>4,5</sub> Im), 5.36 (m, 2H, NCH), 3.48 (s, 12H, CH<sub>3</sub> S-DMSO), 2.31 (m, 2H, CH<sub>2</sub><sup>Pentyl</sup>), 1.81 (m, 2H, CH<sub>2</sub><sup>Pentyl</sup>), 1.74 (m, 4H, CH<sub>2</sub><sup>Pentyl</sup>), 1.69 (m, 2H, CH<sub>2</sub><sup>Pentyl</sup>), 1.64 (s, 6H, CH<sub>2</sub><sup>Pentyl</sup>) ppm. <sup>13</sup>C NMR (100 MHz, CDCl<sub>3</sub>):  $\delta$  = 138.3 (Im-C<sub>2</sub>), 118.5 (Im-C<sub>4,5</sub>), 60.8 (CHN), 46.1 (CH<sub>3</sub>-S-dmsO), 33.5 (CH<sub>2</sub><sup>Pentyl</sup>), 24.0 (CH<sub>2</sub><sup>Pentyl</sup>) ppm. EPR: no signal was observed.

### 2.4.2. Complex **2b**

[RuCl<sub>2</sub>(S-dmsO)<sub>3</sub>(O-dmsO)] complex (350 mg, 0.72 mmol), NHC **1b** (233 mg, 1 mmol), and THF (50 mL) afforded 374 mg (81%) of the title

complex as a yellow solid: anal. calculated for C<sub>19</sub>H<sub>36</sub>Cl<sub>2</sub>N<sub>2</sub>O<sub>2</sub>RuS<sub>2</sub> was 40.71C, 6.47H and 5.00% N; found: 40.92C, 6.54H and 4.88% N. (a) UV-vis:  $\lambda_{\max(n)}$  (nm),  $\epsilon_{\max(n)}$  [M<sup>-1</sup> cm<sup>-1</sup>]:  $\lambda_{\max(1)}$  (245),  $\epsilon_{\max(1)}$  [8437];  $\lambda_{\max(2)}$  (355),  $\epsilon_{\max(2)}$  [651]; (b) FTIR (CsI):  $\nu_x$  (cm<sup>-1</sup>):  $\nu_{C=C}$  (1552),  $\nu_{C=N}$  (1644),  $\nu_{S=O}$  (1102, 1018),  $\nu_{Ru-S}$  (428); (c) <sup>1</sup>H NMR (400 MHz, CDCl<sub>3</sub>):  $\delta$  = 7.17 (s, 2H, CH<sub>4,5</sub> Im), 5.02 (m, 2H, NCH), 3.53 (s, 12H, CH<sub>3</sub> S-DMSO), 2.21 (m, 2H, CH<sub>2</sub><sup>Hexyl</sup>), 1.86 (m, 4H, CH<sub>2</sub><sup>Hexyl</sup>), 1.76 (s, 6H, CH<sub>2</sub><sup>Hexyl</sup>), 1.56 (m, 10H, CH<sub>2</sub><sup>Hexyl</sup>) ppm. <sup>13</sup>C NMR (100 MHz, CDCl<sub>3</sub>):  $\delta$  = 137.5 (Im-C<sub>2</sub>), 117.9 (Im-C<sub>4,5</sub>), 58.7 (CHN), 46.1 (CH<sub>3</sub>-S-dmsO), 33.4 (CH<sub>2</sub><sup>hexyl</sup>), 24.9 (CH<sub>2</sub><sup>hexyl</sup>) ppm. EPR: no signal was observed.

### 2.4.3. Complex **2c**

[RuCl<sub>2</sub>(S-dmsO)<sub>3</sub>(O-dmsO)] complex (350 mg, 0.72 mmol), NHC **1c** (261 mg, 1 mmol), and THF (50 mL) afforded 375 mg (78%) of the title complex as a yellow solid: anal. calculated for C<sub>21</sub>H<sub>40</sub>Cl<sub>2</sub>N<sub>2</sub>O<sub>2</sub>RuS<sub>2</sub> was 41.85C, 6.85H and 4.76% N; found: 42.02C, 6.98H and 4.63% N (a) UV-vis:  $\lambda_{\max(n)}$  (nm),  $\epsilon_{\max(n)}$  [M<sup>-1</sup> cm<sup>-1</sup>]:  $\lambda_{\max(1)}$  (244),  $\epsilon_{\max(1)}$  [4239];  $\lambda_{\max(2)}$  (360),  $\epsilon_{\max(2)}$  [291]; (b) FTIR (CsI):  $\nu_x$  (cm<sup>-1</sup>):  $\nu_{C=C}$  (1549),  $\nu_{C=N}$  (1651),  $\nu_{S=O}$  (1102, 1017),  $\nu_{Ru-S}$  (428); (c) <sup>1</sup>H NMR (400 MHz, CDCl<sub>3</sub>):  $\delta$  = 7.16 (s, 2H, CH<sub>4,5</sub> Im), 5.00 (m, 2H, NCH), 3.56 (s, 12H, CH<sub>3</sub> S-DMSO), 1.92–1.82 (m, 4H, CH<sub>2</sub><sup>Heptyl</sup>), 1.83–1.75 (m, 6H, CH<sub>2</sub><sup>Heptyl</sup>), 1.74–1.70 (m, 6H, CH<sub>2</sub><sup>Heptyl</sup>), 1.66–1.57 (m, 8H, CH<sub>2</sub><sup>Heptyl</sup>) ppm. <sup>13</sup>C NMR (100 MHz, CDCl<sub>3</sub>): <sup>13</sup>C NMR (100 MHz, CDCl<sub>3</sub>):  $\delta$  = 136.9 (Im-C<sub>2</sub>), 118.3 (Im-C<sub>4,5</sub>), 61.5 (CHN), 46.1 (CH<sub>3</sub>-S-dmsO), 35.8 (CH<sub>2</sub><sup>heptyl</sup>), 27.2 (CH<sub>2</sub><sup>heptyl</sup>), 24.0 (CH<sub>2</sub><sup>heptyl</sup>) ppm. EPR: no signal was observed.

### 2.4.4. Complex **2d**

[RuCl<sub>2</sub>(S-dmsO)<sub>3</sub>(O-dmsO)] complex (350 mg, 0.72 mmol), NHC **1d** (289 mg, 1 mmol), and THF (50 mL) afforded 352 mg (70%) of the title complex as a yellow solid: anal. calculated for C<sub>23</sub>H<sub>44</sub>Cl<sub>2</sub>N<sub>2</sub>O<sub>2</sub>RuS<sub>2</sub> was 44.79C, 7.19H and 4.54% N; found: 45.02C, 7.31H and 4.44% N. (a) UV-vis:  $\lambda_{\max(n)}$  (nm),  $\epsilon_{\max(n)}$  [M<sup>-1</sup> cm<sup>-1</sup>]:  $\lambda_{\max(1)}$  (244),  $\epsilon_{\max(1)}$  [7100];  $\lambda_{\max(2)}$  (336),  $\epsilon_{\max(2)}$  [1013]; (b) FTIR (CsI):  $\nu_x$  (cm<sup>-1</sup>):  $\nu_{C=C}$  (1548),  $\nu_{C=N}$  (1638),  $\nu_{S=O}$  (1102, 1025),  $\nu_{Ru-S}$  (428); (c) <sup>1</sup>H NMR (400 MHz, CDCl<sub>3</sub>):  $\delta$  = 7.14 (s, 2H, CH<sub>4,5</sub> Im), 5.05 (m, 2H, NCH), 3.56 (s, 12H, CH<sub>3</sub> S-DMSO), 2.13–2.04 (m, 6H, CH<sub>2</sub><sup>Octyl</sup>), 2.03–1.95 (m, 6H, CH<sub>2</sub><sup>Octyl</sup>), 1.74–1.65 (m, 8H, CH<sub>2</sub><sup>Octyl</sup>), 1.64–1.55 (m, 8H, CH<sub>2</sub><sup>Octyl</sup>) ppm. <sup>13</sup>C NMR (100 MHz, CDCl<sub>3</sub>):  $\delta$  = 136.7 (Im-C<sub>2</sub>), 118.6 (Im-C<sub>4,5</sub>), 60.8 (CHN), 46.1 (CH<sub>3</sub>-S-dmsO), 33.7 (CH<sub>2</sub><sup>octyl</sup>), 26.4 (CH<sub>2</sub><sup>octyl</sup>), 25.4 (CH<sub>2</sub><sup>octyl</sup>), 23.8 (CH<sub>2</sub><sup>octyl</sup>) ppm. EPR: no signal was observed.

## 2.5. Computational details

The structure of the compounds under study were optimized and had their vibrational frequencies calculated using the density functional theory (DFT) at the level of the functional M06 [31], implemented in Gaussian 09 [32], using the basis set DGDZVP [33]. The structures were solvated using the IEFPCM model [34].

## 2.6. ROMP procedure

In a typical ROMP experiment, 1.1  $\mu$ mol of complex was dissolved in CH<sub>2</sub>Cl<sub>2</sub> (2 mL) with an appropriate amount of monomer (NBE, 5.5 mmol), followed by addition of carbene source (EDA, 31  $\mu$ mol). The reaction mixture was stirred up to 60 min at 50 °C in a silicon oil bath. At room temperature, 5 mL of methanol was added and the polymer was filtered, washed with methanol and dried in a vacuum oven at 40 °C up to constant weight. The reported yields are average values from catalytic runs performed at least three times with 10% error at the most. The isolated polyNBEs were dissolved in THF for GPC data.

## 2.7. ATRP procedure

In a typical ATRP experiment, 12.3  $\mu$ mol of complex was placed in a

Schlenk tube containing a magnet bar and capped by a rubber septum. Air was expelled by three vacuum–nitrogen cycles before appropriate amounts of monomer (MMA, 12.3 mmol), initiator (EBiB, 24.6  $\mu$ mol), and toluene (1 mL) were added. All liquids were handled with dried syringes under nitrogen. The tube was capped under N<sub>2</sub> atmosphere using Schlenk techniques, then the reaction mixture was immediately immersed in an oil bath previously heated to the desired temperature. The polymerizations were conducted at 85 °C. The samples were removed from the tube after certain time intervals using degassed syringes. The polymerization was stopped when the reaction mixture became very viscous. The reported conversions are average values from catalytic runs performed at least twice.

### 3. Results and discussion

#### 3.1. Synthesis and characterization

The one-pot procedure described for 1,3-dicyclohexylimidazolium tetrafluoroborate could be seamlessly translated to the preparation of 1,3-dicycloalkylimidazolium tetrafluoroborate (**1a**, **1c**, and **1d**) from glyoxal, cycloalkylamine (cyclopentylamine, cycloheptylamine, and cyclooctylamine), paraformaldehyde, and tetrafluoroboric acid [29,30]. This synthesis protocol of NHC ligands **1a–1d** is an optimized route from the procedure reported by Nolan and co-workers, while searching for bulky NHC ligands to coordinate in transition metal catalysts [35–40]. The corresponding products were obtained under mild conditions; their confirmation was demonstrated by spectroscopic data (Scheme 1). The ligands **1a–1d** are stable, non-hygroscopic solid that could be easily purified by recrystallization from isopropanol with typical yields of 70%.

Prior to the complexation step, these NHC precursors were suspended in dry THF and deprotonated with sodium hydride in the presence of a catalytic amount of potassium *tert*-butoxide at room temperature. Within 2 h, the initially white solution became progressively pale yellow. Once the deprotonation step was completed, the suspensions were allowed to settle down and the inorganic byproduct was filtered off, along with any unreacted starting materials. The deprotonated imidazolium salts **1a–1d** were reacted with an equimolar amount of [RuCl<sub>2</sub>(S-dmsO)<sub>3</sub>(O-dmsO)] complex to obtain the NHC ruthenium(II) complexes **2a–2d** in high yields (Scheme 2). The complexes **2a–2d** were formed only in the powder form and non-hygroscopic, which was not suitable for single X-ray diffraction analysis. Further attempts to get crystals were not successful.

ESR spectra of the isolated compounds were silent and elemental analyses suggest five-coordinated complexes with the general formula the [RuCl<sub>2</sub>(dmsO)<sub>2</sub>(NHC)]; where NHC = 1,3-dicycloalkylimidazolium **1a–1d**. Each ruthenium centre presents low spin d<sup>6</sup> electronic configuration with +2 oxidation state.

The infrared spectra were similar, with two strong bands in the

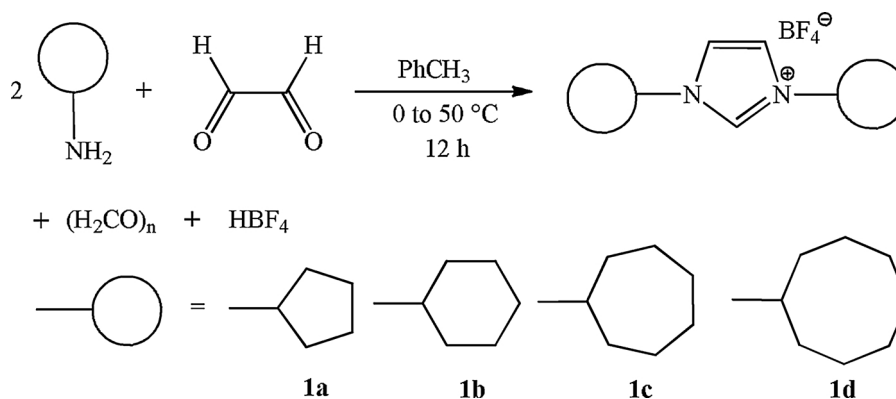
region of 1102–1018 cm<sup>-1</sup> assigned to the  $\nu$ (S=O) stretching vibrations. S-bonded dmsO was evident from Ru–S stretching in 428 cm<sup>-1</sup>. These bands now support linkage of dmsO to the ruthenium metal centre through sulphur, following the literature [28,41,42]. Bands in 1548–1552 cm<sup>-1</sup> were attributed to  $\nu$ (C=C) of the imidazole ring. The bands in the region of 345 and 310 cm<sup>-1</sup> were attributed to  $\nu$ (Ru–Cl) asymmetric and symmetric stretching vibrations, respectively, suggesting two *cis*-positioned Cl<sup>-</sup> ligands.

In the <sup>1</sup>H NMR spectra in CDCl<sub>3</sub> for the synthesized ligands (**1a–1d**) and their complexes (**2a–2d**) are given in the experimental section. The peaks in the range 1.0–2.5 ppm for ligands **1a–1d** and complexes **2a–2d**, as multiplets, are assignable to the CH<sub>2</sub> groups hydrogens from the *N*-cycloalkyl substituent. The singlet at 3.5 ppm is assigned to the methyl groups of the S-bonded dmsO. This signal indicated two equivalent S-dmsO molecules *trans*-positioned to two Cl<sup>-</sup> ligands in the complexes **2a–2d**. Additionally, the peaks at range 4.0–5.0 ppm for ligands **1a–1d** and around 5.3 ppm for complexes **2a–2d**, as quintuplets, are assignable to the hydrogen attached to the carbon which connects the cycloalkyl substituent to the imidazole nitrogen. In the <sup>1</sup>H NMR spectra of ligands **1a–1d** and complexes **2a–2d**, the chemical shifts observed around 7.2–7.5 ppm for free ligands and at 7.0–7.2 ppm for complexes **2a–2d** as singlets are assigned to the hydrogens present in the carbon double bond of the imidazole ring. Finally, the signal at 8.8–9.0 ppm refers to the hydrogen of the C<sub>2</sub> carbon of the imidazole ring in the free ligands **1a–1d**. These signals did not appear in the complexes **2a–2d** as expected, confirming NHC carbene coordination to the ruthenium centre. In the <sup>13</sup>C NMR spectra, the carbon peaks between 23.7–134.3 ppm for ligands **1a–1d** and 24.0–138.3 ppm for complexes **2a–2d** were observed.

Correlating the NMR data with the FTIR spectrum, which suggested that the two chloride ligands are *cis*-positioned, a square pyramidal geometry is assigned to Ru(II) centre in all complexes synthesized.

Electronic spectra of ligands **1a–1d** (Fig. S1) and their complexes (Fig. 2) have been recorded in the 200–700 nm range in CH<sub>2</sub>Cl<sub>2</sub>. The formation of the complexes **2a–2d** was also confirmed by electronic spectra. In the electronic spectra of the complexes **2a–2d** show a band around 242 nm corresponding to intra-ligand  $\pi \rightarrow \pi$  transition and another band of lower energy in the region 324 nm assignable to MLCT transition. The bands assigned to intra-ligand  $\pi \rightarrow \pi$  transition show hypsochromic shifts relative to their free ligands. This displacement of the absorption bands of the complexes **2a–2d** most likely originate from the metalation which increases the conjugation and delocalization of the whole electronic system and results in the energy change of the  $\pi \rightarrow \pi$  transition of the conjugated chromophore. These results clearly indicate that the ligand coordinates to metal centre, which are in accordance with the results of the other spectroscopic data.

The electrochemical activity of the complexes **2a–2d** was studied by cyclic voltammetry in scan rate of 100 mV s<sup>-1</sup> in CH<sub>2</sub>Cl<sub>2</sub> solution containing 0.1 M *n*-Bu<sub>4</sub>NPF<sub>6</sub> supporting electrolyte in the potential range 300–1100 mV. Under these conditions the redox potential ( $E_{1/2}$ )



Scheme 1. Synthesis protocol of NHC ligands **1a–1d**.



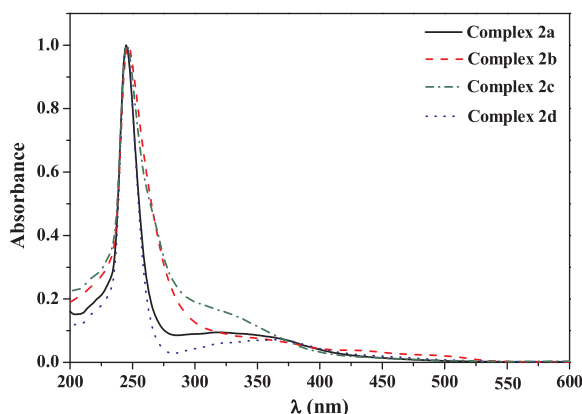
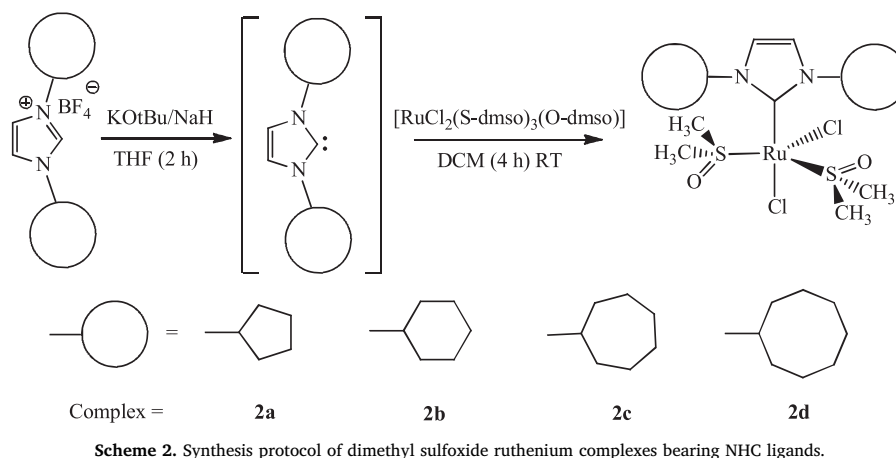


**Fig. 2.** Electronic spectra of the complexes **2a–2d** in degassed  $\text{CH}_2\text{Cl}_2$  solution at room temperature ( $[\text{Ru}] = 0.1 \text{ mmol L}^{-1}$ ).

**Table 1**  
Cyclic voltammetry<sup>[a]</sup> results for complexes **2a–2d**.

Complex	CV			
	$E_{pa}$ (mV)	$E_{pc}$ (mV)	$E_{1/2}$ (mV)	$\Delta E_p$ (mV)
<b>2a</b>	726	641	683	85
<b>2b</b>	720	658	694	62
<b>2c</b>	695	616	655	79
<b>2d</b>	723	649	686	74

for the  $\text{Fc}/\text{Fc}^+$  couple occurred at 465 mV, with  $\Delta E_p = 208 \text{ mV}$  (Fig. S2); the electrochemical data of the complexes **2a–2d** are given in Table 1 and the representative cyclic voltammograms for the behaviours of the complexes are shown in Fig. 3. All the four NHC ruthenium complexes exhibit identical one-electron response corresponding to the  $\text{Ru}^{\text{II/III}}$  redox process in the 420–460 mV range versus  $\text{Ag}/\text{AgCl}$ . Their peak-to-peak separations ( $\Delta E_p$ ) are lower to the ferrocene-ferrocenium couple, indicating that these  $\text{Ru}^{\text{II}}/\text{Ru}^{\text{III}}$  couples are facile and reversible. The  $\Delta E_p$  values are somewhat larger than the canonical value for ideal Nernstian behavior (59 mV), indicating some reorganization of the coordination sphere of the ruthenium centre. This may reflect preferred coordination geometries for each redox state,  $\text{Ru}^{\text{II}}$ ,  $d^6$  and  $\text{Ru}^{\text{III}}$ ,  $d^5$ . Lower oxidation potential values for complexes **2a–2d** were obtained as compared with precursor  $[\text{RuCl}_2(\text{S-dmsO})_3(\text{O-dmsO})]$  ( $E_{ox} = 1520 \text{ mV}$  versus  $\text{Ag}/\text{AgCl}$ ) and were associated with the occurrence of strong NHC  $\sigma$ -donation that destabilizes the HOMO orbital in the ground state in each case.

<sup>[a]</sup>Conditions:  $\text{CH}_2\text{Cl}_2$ ,  $n\text{-Bu}_4\text{NPF}_6$  (supporting electrolyte,  $0.1 \text{ mol L}^{-1}$ ),  $[\text{Ru}] = 5 \text{ mmol L}^{-1}$ , scan rate =  $100 \text{ mV s}^{-1}$ , platinum

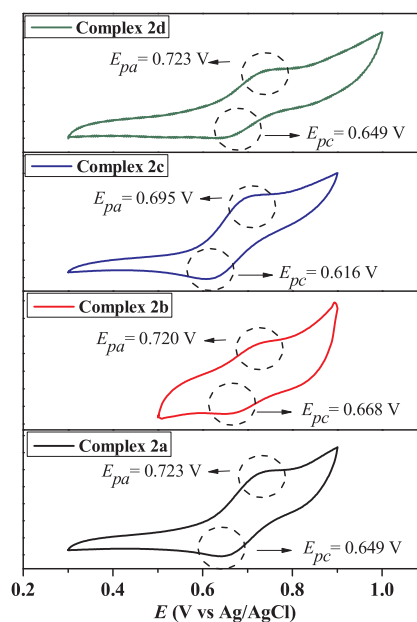


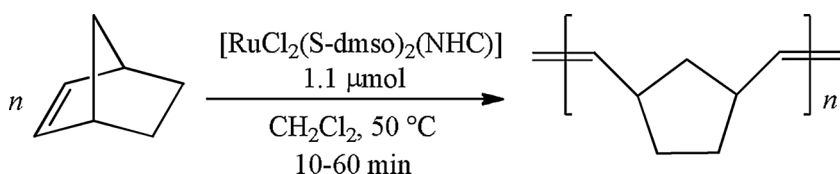
**Fig. 3.** Cyclic voltammograms of **2a–2d** in  $\text{CH}_2\text{Cl}_2$  at  $25^\circ\text{C}$ .  $[\text{Ru}] = 10 \text{ mM}$ ;  $[n\text{-Bu}_4\text{NPF}_6] = 0.1 \text{ M}$ . Scanning anodically from 0.3 up to 1.0 V at scan rate of  $100 \text{ mV s}^{-1}$ .

disk and wire (working and auxiliary electrode),  $\text{Ag}/\text{AgCl}$  (reference electrode).  $E_{1/2}$  is the half-potential for the complex;  $\Delta E_p$  is the cathodic-anodic peak separation.

### 3.2. ROMP reactions

In order to assess the catalytic efficiency of dimethyl sulfoxide ruthenium(II) complexes **2a–2d**, ROMP of norbornene (NBE) was attempted in  $\text{CH}_2\text{Cl}_2$  at  $50^\circ\text{C}$  with a  $[\text{NBE}]/[\text{Ru}]$  ratio of 5000 (Scheme 3). Under these conditions, complexes **2a–2d** were completely inefficient. In contrast, when ethyl diazoacetate (EDA) was added to generate metathetically active ruthenium–carbene species from  $[\text{RuCl}_2(\text{S-dmsO})_2(\text{NHC})]$  precursors **2a–2d**, ROMP occurred with moderate yields.

Fig. 4 shows the variation in the yield values of the isolated polymers as a function of time, in which an increase of the yield with increase of the polymerization time is observed for all the evaluated complexes. Initially, the catalytic activity of the complexes studied (**2a–2d**) in ROMP of NBE was expected to increase as the number of  $\text{CH}_2$  groups increased in the cycloalkyl substituents, believing that  $\text{NHC} \rightarrow \text{Ru} \rightarrow \text{olefin}$  synergism would be favored for more efficient activation of the olefin (NBE). However, the catalytic activity of these complexes for ROMP of NBE showed an inverse behavior, in which it increased from



Scheme 3. ROMP of NBE catalysed by Ru-dmsco complexes.

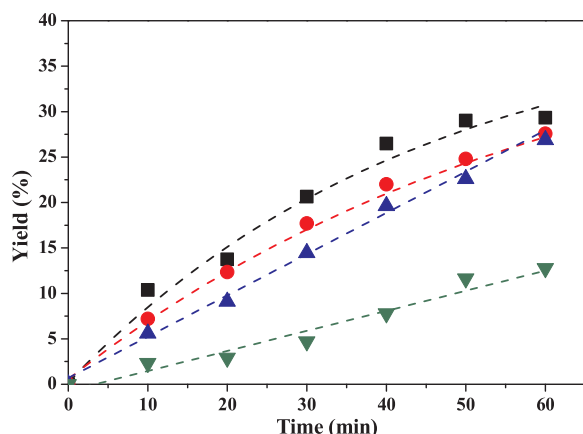


Fig. 4. Dependence of yield as a function of time for ROMP of NBE with **2a** (■), **2b** (●), **2c** (▲) and **2d** (▼); [NBE]/[Ru] = 5000 and [EDA]/[Ru] = 28 in CH<sub>2</sub>Cl<sub>2</sub> at 50 °C.

the complex **2d** (cyclooctyl) to complex **2a** (cyclopentyl). We believe that this order of reactivity of the complexes may be associated with a kinetic dependence in the initiation step. Since pre-catalysts **2a-2d** are

five-coordinated complexes, the success of ROMP requires the labilization of a *cis*-positioned ligand to the metal-carbene. In order to better understand the mechanism of the initiation step, the ROMP of NBE with complexes **2a-2d** was performed in the presence of excess dmsco ligand (5 μL of EDA with [NBE]/[dmsco]/[Ru] = 5000/20/1 for 60 min at 50 °C), in which no polyNBE yield was observed. This inertia indicates that the initiation step involves S-dmsco loss from the ruthenium centre.

A computational investigation was carried out to explain the difference of activity between complexes **2a-2d** in ROMP reactions. Fig. 5 shows the equilibrium position of the monomer from the ruthenium centre; as the number of CH<sub>2</sub> groups in the cycloalkyl substituents increases, the equilibrium distance Ru–NBE increases: 2.421, 2.448, 2.448, and 2.452 Å for **2a**, **2b**, **2c** and **2d**, respectively. The displacement of the dmsco molecule from the ruthenium can be favored by the increase in the cycloalkyl group, however, nucleophilic attack of the NBE at the Ru centre is disfavored by increasing the cycloalkyl group due to steric reasons, which explains the decrease of the yield values in the following order: **2d** < **2c** < **2b** < **2a**. Further, an analysis of the molecular orbitals shows that there is no significant electronic density on the cycloalkanes and that their main role is in directing the approximation of the NBE to the ruthenium centre.

The NHC → Ru → S-dmsco synergism makes the initiation step very

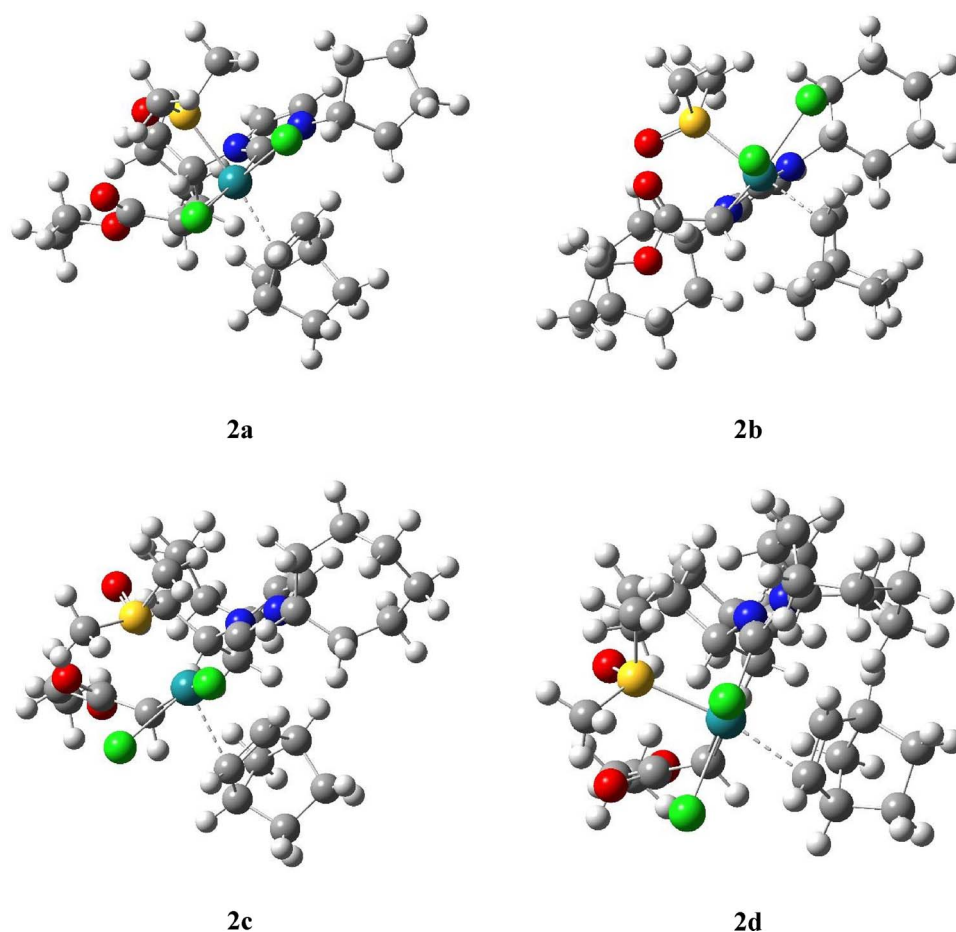


Fig. 5. Representation of EDA and NBE coordinated to the precursor complexes **2a-2d**.

**Table 2**

Yield values and SEC data from the ROMP of NBE with **2a-2d** at 50 °C; [NBE]/[Ru] = 5000 and [EDA]/[Ru] = 28 with 1.1 μmol of complex in CH<sub>2</sub>Cl<sub>2</sub>.

Complex	Time (min)	Yield (%)	M <sub>n</sub> (10 <sup>3</sup> g mol <sup>-1</sup> )	PDI
<b>2a</b>	10	10.3	2.4	1.63
	20	13.7	4.5	2.78
	30	20.6	4.2	3.11
	40	26.5	4.1	3.16
	50	29.0	4.0	3.17
	60	29.3	5.4	3.98
<b>2b</b>	10	7.2	4.0	2.57
	20	12.3	5.7	2.74
	30	17.7	4.3	3.50
	40	22.0	5.1	3.43
	50	24.8	4.5	3.54
	60	27.6	5.2	3.19
<b>2c</b>	10	5.6	2.2	1.66
	20	9.1	2.4	2.14
	30	14.5	2.8	2.24
	40	19.6	3.1	2.55
	50	22.6	3.9	3.17
	60	26.9	3.3	3.27
<b>2d</b>	10	2.3	3.8	1.82
	20	2.9	5.5	2.73
	30	4.7	4.6	2.28
	40	7.8	5.1	2.86
	50	11.6	4.3	2.62
	60	12.8	5.1	3.01

slow, producing polyNBE with large dispersity. The PDI values of about 3.0 may be associated with a possible inefficiency of the initiation step; in other words, the great synergism becomes detrimental because the coordination of the olefin (NBE) to the ruthenium centre depends on the dmsoligand loss which should be fast and uniform. Consequently, chain growth occurs before all Ru units have initiated the ROMP reactions. In this way, a large dispersion in the size of the polymer chains was obtained. Although the PDI values were large, the isolated polyNBEs showed monomodal molecular weight distributions with molar weights in the range of  $2.2 \times 10^3$  to  $5.7 \times 10^3$  g mol<sup>-1</sup> (Table 2).

Based on this, it is possible to infer that the difference in the reactivity of the complexes studied is directly related to the steric characteristics of the NHC ligands, which are modulated by their substituents (cycloalkyl groups). Upon metal-carbene formation, a S-dmsoligand leaves the complex, followed by the coordination of NBE to the carbene-Ru species. This associative pathway was confirmed by theoretical calculations. The formation of the Ru-EDA complex without the output of a dmsoligand is slightly favored (about 22 kJ/mol) in comparison with a dissociative mechanism. Further, the polymerization in the presence of dmsoligand confirmed that the ROMP reaction did not occur, although the carbene complex formation took place. The ROMP will only occur when the dmsoligand undergoes discoordination from the metal centre (Scheme 4).

### 3.3. ATRP reactions

Next, we focused our attention on the atom-transfer radical polymerization (ATRP) of methyl methacrylate (MMA) initiated by ethyl-2-bromoisobutyrate (Scheme 5). The complexes **2a-2d** have properties that make them promising compounds for use as ATRP catalysts. They provide reversible or quasi-reversible Ru<sup>II</sup>/Ru<sup>III</sup> couples at easily accessible potentials, as shown by the electrochemical data. They are five-coordinate complexes with square pyramidal geometry, which makes it possible for a halide ligand to enter the coordination sphere. The polymerization of MMA via ATRP with complexes **2a-2d** were performed as a function of time using a [MMA]/[EBiB]/[Ru] ratio of 1000/2/1 molar ratio at 85 °C.

The MMA conversion values increase linearly as a function of time in all cases (Fig. 6). The catalytic activity of the complexes **2a-2d** has increased with the increase of the CH<sub>2</sub> groups on the cycloalkyl substituent. The complex **2a** achieved a maximum conversion of 47% of polyMMA, and almost doubled with **2d**, reaching 80% in 12 h.

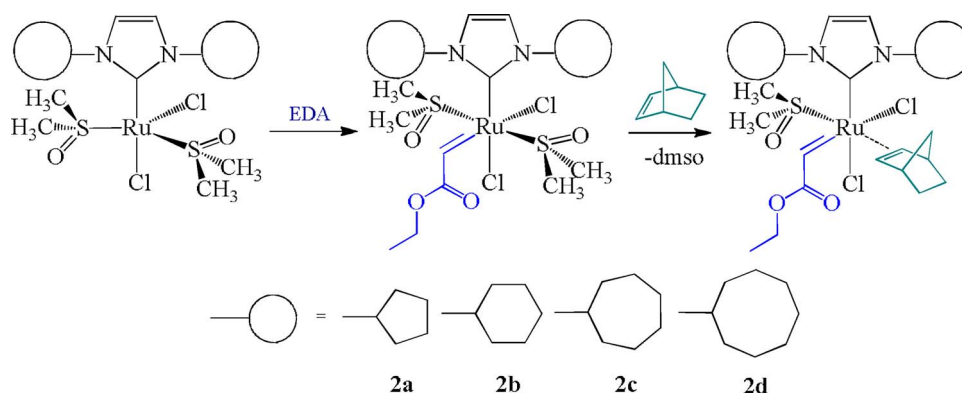
Kinetics studies of the polymerization of MMA mediated by the complexes **2a-2d** show a linear correlation of ln([MMA]<sub>0</sub>/[MMA]) as a function of time ( $r^2 = 0.992, 0.985, 0.990, \text{ and } 0.994$  for **2a, 2b, 2c,** and **2d**, respectively) (Fig. 7). This linearity clearly indicates that the concentration of radicals remains constant during the polymerization of MMA. The slope in the first-order kinetic plots allowed us to calculate the kinetic constants of reactions mediated by each one of the complexes ( $1.52 \times 10^{-5} \text{ s}^{-1}$  for **2a**,  $2.29 \times 10^{-5} \text{ s}^{-1}$  for **2b**,  $2.73 \times 10^{-5} \text{ s}^{-1}$  for **2c**, and  $3.70 \times 10^{-5} \text{ s}^{-1}$  for **2d**).

In this case, unlike the ROMP reactions, the catalytic activity of the complexes studied follows this trend: **2a** < **2b** < **2c** < **2d**, it is believed that the strong σ-donation of NHC → Ru favors the activation step in ATRP (reaction between the catalyst and initiator or dormant species). This order of reactivity observed indicates that the ATRP mechanism mediated by the complexes **2a-2d** does not appear to involve the lability of S-dmsoligand from the coordination sphere.

The linear semilogarithmic plot of ln([MMA]<sub>0</sub>/[MMA]) versus time and the linear increase of molecular weight with conversion, in conjunction with moderate PDIs (Table 3), illustrates a certain level of control imparted by the complexes **2a-2d** (Figs. 7 and 8). However, in repeated kinetic experiments molecular weights were observed to be much higher than the theoretical values, thereby revealing a low initiation efficiency. This is associated to the number of growing radical chains being lower than expected, resulting in an effective increase in the monomer concentration.

## 4. Conclusions

Four *N*-heterocyclic carbene **1a-1d** and their respective complexes RuCl<sub>2</sub>(S-dmsoligand)(IPent) (**2a**), [RuCl<sub>2</sub>(S-dmsoligand)<sub>2</sub>(IHex)] (**2b**), [RuCl<sub>2</sub>(S-dmsoligand)<sub>2</sub>(IHept)] (**2c**), and [RuCl<sub>2</sub>(S-dmsoligand)<sub>2</sub>(IOct)] (**2d**) were



**Scheme 4.** Illustration of possible reaction steps for ROMP of NBE with the complexes **2a-2d**.

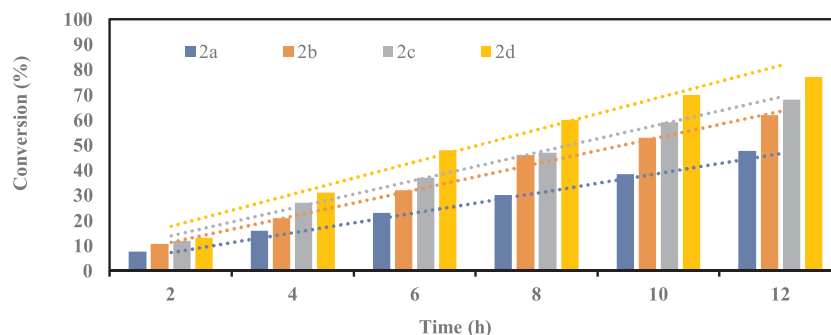
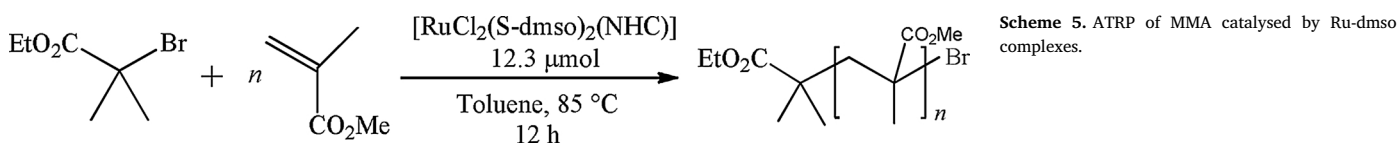


Fig. 6. Dependence of conversion on the reaction time for ATRP of MMA with 2a-2d; [MMA]/[EBiB]/[Ru] = 1000/2/1 with 12.3  $\mu\text{mol}$  of complex in toluene at 85  $^\circ\text{C}$ .

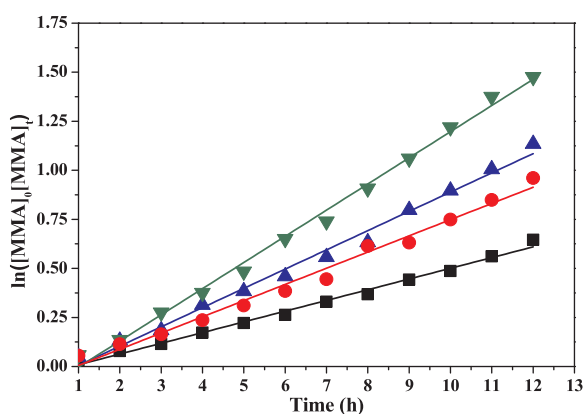


Fig. 7. Dependence of  $\ln([\text{MMA}]_0/[\text{MMA}])$  on the reaction time for ATRP of MMA with 2a (■), 2b (●), 2c (▲) and 2d (▼); [MMA]/[EBiB]/[Ru] = 1000/2/1 with 12.3  $\mu\text{mol}$  of complex in toluene at 85  $^\circ\text{C}$ .

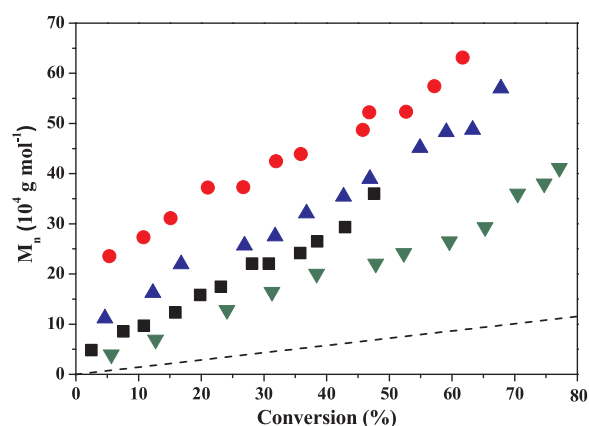


Fig. 8. Dependence of  $M_n$  and PDI on the conversion for ATRP of MMA with 2a (■), 2b (●), 2c (▲) and 2d (▼); [MMA]/[EBiB]/[Ru] = 1000/2/1 with 12.3  $\mu\text{mol}$  of complex in toluene at 85  $^\circ\text{C}$ .  $M_{n(\text{theor})}$  (black dashed-line).

Table 3

Conversion values and GPC data from the ATRP of MMA with 2a-2d; [MMA]/[EBiB]/[Ru] = 1000/2/1 with 12.3  $\mu\text{mol}$  of complex in toluene at 85  $^\circ\text{C}$ .

Complex	Time (h)	Conversion (%)	$M_n$ ( $10^4 \text{ g mol}^{-1}$ )	PDI
2a	2	7.6	8.5	1.92
	4	15.9	12.3	1.79
	6	23.1	17.4	1.68
	8	30.8	22.0	1.66
	10	38.5	26.4	1.62
	12	47.6	36.0	1.45
2b	2	10.8	27.3	1.43
	4	21.0	37.2	1.38
	6	31.9	42.4	1.36
	8	45.8	48.7	1.31
	10	52.7	52.3	1.20
	12	61.7	63.1	1.17
2c	2	12.3	16.2	1.31
	4	26.9	25.6	1.21
	6	36.8	32.1	1.15
	8	46.9	38.9	1.10
	10	59.1	48.2	1.10
	12	67.8	56.9	1.10
2d	2	12.7	6.9	1.32
	4	31.3	16.4	1.22
	6	47.8	22.0	1.17
	8	59.6	26.4	1.13
	10	70.5	36.0	1.10
	12	77.1	41.1	1.09

successfully synthesized. Ligands **1a-1d** were characterized by infrared, UV-vis and  $^1\text{H}$  and  $^{13}\text{C}$  NMR spectroscopy, whereas complexes **2a-2d** were characterized by infrared, UV-vis and  $^1\text{H}$  and  $^{13}\text{C}$  NMR spectroscopy, elementary analysis, and cyclic voltammetry. It was concluded that two DMSO molecules have been replaced by a *N*-heterocyclic carbene in the coordination sphere, leading to five-coordinated complexes.

The complexes **2a-2d** demonstrated moderate catalytic activities as catalytic precursors in ROMP of NBE at 50  $^\circ\text{C}$  with [NBE]/[Ru] ratio of 5000 in the presence of 5  $\mu\text{L}$  of EDA for 5–60 min. The catalytic activity of complexes **2a-2d** in ROMP increased as the  $\text{CH}_2$  group decreased in the cycloalkyl substituents, that means from **2d** to **2a**. This order of reactivity is associated with a kinetic dependence at the initiation step, which the departure of the S-dmsO ligand from the metal centre is involved in the rate limiting step of the reaction. The electronic synergism induced by the strong  $\sigma$ -donation of the NHC and the  $\pi$ -acceptor S-dmsO (NHC  $\rightarrow$  Ru  $\rightarrow$  S-dmsO) contributed to the stability of the complexes **2a-2d**. The nucleophilic attack of the NBE at the Ru centre is disfavored by increasing the cycloalkyl group due to steric reasons, which explains the decrease of the yield values in the following order: **2d** < **2c** < **2b** < **2a**.

The polymerization of MMA mediated by the complexes **2a-2d** was performed using a [MMA]/[EBiB]/[Ru] = 1000/2/1 molar ratio at 85  $^\circ\text{C}$ . Those complexes display activity as mediators for the controlled radical polymerization of MMA following an ATRP mechanism. The molecular weight of polyMMA increased with conversion, with



decreasing PDI values with all complexes, which illustrates a certain level of control imparted by the complexes **2a–2d**.

### Acknowledgement

The authors are indebted to the financial support from FAPESP (Proc. 2013/10002-0).

### Appendix A. Supplementary data

Supplementary data associated with this article can be found, in the online version, at <http://dx.doi.org/10.1016/j.mcat.2018.01.032>.

### References

- [1] R.H. Crabtree, *The Organometallic Chemistry of the Transition Metals*, Wiley, New York, 1988.
- [2] L.A. Thompson, J. Ellman, *Chem. Rev.* 96 (1996) 555–560.
- [3] D.L. Boger, W. Chai, Q. Jin, *J. Am. Chem. Soc.* 120 (1998) 7220–7225.
- [4] K.V. Bernaerts, F.E. Du Prez, *Prog. Polym. Sci.* 31 (2006) 671–722.
- [5] V. Dragutan, I. Dragutan, *J. Organomet. Chem.* 691 (2006) 5129–5147.
- [6] Y. Yagci, M.A. Tasdelen, *Prog. Polym. Sci.* 31 (2006) 1133–1170.
- [7] R.G. Lopez, F. D'Agosto, C. Boisson, *Prog. Polym. Sci.* 32 (2007) 419–454.
- [8] J.B. Matson, R.H. Grubbs, *Macromolecules* 41 (2008) 5626–5631.
- [9] G. Morandi, S. Piogé, S. Pascual, *Mater. Sci. Eng. C* 29 (2009) 367–371.
- [10] D.E. Fogg, E.N. Dos Santos, *Coord. Chem. Rev.* 248 (2004) 2365–2379.
- [11] C.W. Bielawski, R.H. Grubbs, *Prog. Polym. Sci.* 32 (2007) 1–29.
- [12] K. Nomura, M.M. Abdellatif, *Polymer* 51 (2010) 1861–1881.
- [13] D. Yang, W. Huang, J.H. Yu, J.S. Jiang, L.Y. Zhang, M.R. Xie, *Polymer* 51 (2010) 5100–5106.
- [14] L.C. So, S. Faucher, S. Zhu, *Prog. Polym. Sci.* 39 (2014) 1196–1234.
- [15] F. di Lenna, K. Matyjaszewski, *Prog. Polym. Sci.* 35 (2010) 959–1021.
- [16] M. Kamigaito, *J. Polym.* 43 (2011) 105–120.
- [17] F. Simal, S. Delfosse, A. Demonceau, A.F. Noels, K. Denk, F.J. Kohl, T. Weskamp, W.A. Herrmann, *J. Chem. Eur.* 8 (2002) 3047–3052.
- [18] J.M.E. Matos, B.S. Lima Neto, *J. Mol. Catal. A* 222 (2004) 81–85.
- [19] J.M.E. Matos, B.S. Lima Neto, *J. Mol. Catal. A* 259 (2006) 286–291.
- [20] J.L.S. Sá, B.S. Lima Neto, *J. Mol. Catal. A* 304 (2009) 187–190.
- [21] J.L.S. Sá, L.H. Vieira, E.S.P. Nascimento, B.S. Lima Neto, *Appl. Catal. A* 374 (2010) 194–200.
- [22] V.P. Carvalho Jr., C.P. Ferraz, B.S. Lima Neto, *J. Mol. Catal. A* 333 (2010) 46–53.
- [23] H.K. Chaves, C.P. Ferraz, V.P. Carvalho Jr., B.S. Lima Neto, *J. Mol. Catal. A* 385 (2014) 46–53.
- [24] L.R. Fonseca, E.S.P. Nascimento, J.L.S. Sá, B.S. Lima Neto, *New J. Chem.* 39 (2015) 4063–4069.
- [25] R.A.N. Silva, P. Borim, L.R. Fonseca, B.S. Lima Neto, J.L.S. Sá, V.P. Carvalho Jr., *Catal. Lett.* 147 (2017) 1144–1152.
- [26] P. Borim, B.S. Lima Neto, B.E. Goi, V.P. Carvalho Jr., *Inorg. Chim. Acta* 456 (2017) 171–178.
- [27] M.B.A. Afonso, L.G. Gonçalves, P. Borim, B.E. Goi, V.P. Carvalho Jr., *J. Braz. Chem. Soc.* 28 (2017) 1407–1413.
- [28] I.P. Evans, A. Spencer, G. Wilkinson, *J. Chem. Soc. Dalton Trans.* (1973) 204–209.
- [29] R.H. Archer, J.R. Carpenter, S.-J. Hwang, A.W. Burton, C.-Y. Chen, S.I. Zones, M.E. Davis, *Chem. Mater.* 22 (2010) 2563–2572.
- [30] M. Hans, J. Wouters, A. Demonceau, L. Delaude, *J. Chem. Eur.* 21 (2015) 10870–10877.
- [31] Y. Zhao, D.G. Truhlar, *Theor. Chem. Accounts* 120 (2006) 215–241.
- [32] M.J. Frisch, G.W. Trucks, H.B. Schlegel, G.E. Scuseria, M.A. Robb, J.R. Cheeseman, G. Scalmani, V. Barone, B. Mennucci, G.A. Petersson, H. Nakatsuji, M. Caricato, X. Li, H.P. Hratchian, A.F. Izmaylov, J. Bloino, G. Zheng, J.L. Sonnenberg, M. Hada, M. Ehara, K. Toyota, R. Fukuda, J. Hasegawa, M. Ishida, T. Nakajima, Y. Honda, O. Kitao, H. Nakai, T. Vreven, J.A. Montgomery, Jr., J.E. Peralta, F. Ogliaro, M. Bearpark, J.J. Heyd, E. Brothers, K.N. Kudin, V.N. Staroverov, T. Keith, R. Kobayashi, J. Normand, K. Raghavachari, A. Rendell, J.C. Burant, S.S. Iyengar, J. Tomasi, M. Cossi, N. Rega, J.M. Millam, M. Klene, J.E. Knox, J.B. Cross, V. Bakken, C. Adamo, J. Jaramillo, R. Gomperts, R.E. Stratmann, O. Yazyev, A.J. Austin, R. Cammi, C. Pomelli, J.W. Ochterski, R.L. Martin, K. Morokuma, V.G. Zakrzewski, G.A. Voth, P. Salvador, J.J. Dannenberg, S. Dapprich, A.D. Daniels, O. Farkas, J.B. Foresman, J.V. Ortiz, J. Cioslowski, D.J. Fox, Gaussian 09, Revision E.01, Gaussian, Inc., Wallingford CT, 2013.
- [33] N. Godbout, D.R. Salahub, J. Andzelm, E. Wimmer, *Can. J. Chem.* 70 (1992) 560–571.
- [34] J. Tomasi, B. Mennucci, E. Cancès, *J. Mol. Struct. (Theochem.)* 464 (1999) 211–226.
- [35] J. Huang, S.P. Nolan, *J. Am. Chem. Soc.* 121 (1999) 9889–9890.
- [36] P. de Frémont, N. Marion, S.P. Nolan, *Coord. Chem. Rev.* 253 (2009) 862–892.
- [37] N. Marion, S.P. Nolan, *Chem. Soc. Rev.* 37 (2008) 1776–1782.
- [38] S. Díez-González, N. Marion, S.P. Nolan, *Chem. Rev.* 109 (2009) 3612–3676.
- [39] X. Bantreil, S.P. Nolan, *Nat. Protoc.* 6 (2011) 69–77.
- [40] S.P. Nolan, *N-Heterocyclic Carbenes Effective Tools for Organometallic Synthesis*, Wiley-VCH, Weinheim, 2014.
- [41] E. Alessio, *Chem. Rev.* 104 (2004) 4203–4242.
- [42] M. Calligaris, O. Carugo, *Chem. Rev.* 153 (1996) 83–154.